

GPS radio holography as a tool for remote sensing of the atmosphere, mesosphere, and terrestrial surface from space

Alexander Pavelyev · Yuei-An Liou · Christoph Reigber · Jens Wickert

Kiyoshi Igarashi · Klemens Hocke · Cheng-Yung Huang

Abstract GPS radio occultation (RO) signals are highly coherent and precise, and thus sufficient for holographic investigation of the atmosphere, ionosphere, and the Earth's surface from space. In principle, three-dimensional radio-holographic remote sensing is possible by using new radio holographic equations to retrieve the radio field within the atmosphere from a radio field known at some interface outside the atmosphere. A simplified two-dimensional form of the radio-holographic equations which are developed under an assumption of local spherical symmetry can be used to obtain two-dimensional radio images of the atmosphere and terrestrial surface. To achieve this, radio holograms recorded by a GPS receiver onboard a low earth orbit (LEO) satellite at two GPS frequencies can be used and focused synthetic aperture principle applied. Analysis of GPS/MET RO data is presented to show the effectiveness of a radio-holographic approach. It is shown that the amplitude of GPS radio signals (in addition to phase data) can be used to

obtain detailed altitude profiles of the vertical gradient of refractivity in the atmosphere and electron density in the mesosphere. The results demonstrate the applicability of GPS radio holography for a detailed global study of the natural processes in the atmosphere and mesosphere.

Introduction

In this paper the new three-dimensional vector radio-holographic equations are presented. These equations connect the electromagnetic field inside an inhomogeneous volume in space with the electromagnetic field at its boundary. Under an assumption of local spherical symmetry, these equations can be reduced to a two-dimensional scalar case. In the plane scalar case, these equations coincide with a two-dimensional scalar formula introduced early by Vladimirov (1971) to retrieve the electromagnetic field in a plane by using the phase and amplitude of a radio field given on a line located within this plane. Both the three-dimensional vector equations and the two-dimensional scalar formula can be applied for remote sensing from space. We discuss the application of global positioning system (GPS) radio holography to a radio occultation (RO) study of the Earth's atmosphere, mesosphere, and terrestrial surface. Practical testing of the RO method during GPS/MET, SAC-C, and CHAMP experiments showed its strengths for the study of the atmosphere and ionosphere of the Earth (e.g., Ware et al. 1996; Kursinski et al. 1997; Rocken et al. 1997; Hajj and Romans 1998; Feng and Herman 1999; Liou and Huang 2002). However, the RO experiments showed a necessity to derive more accurate and effective scientific methodology to infer the atmospheric, mesospheric and ionospheric parameters and to improve the vertical resolution. Usually the phase data are used to retrieve vertical profiles of the refraction index, temperature in the atmosphere, and electron density in the ionosphere with a vertical resolution of about the size of the Fresnel zone (~0.2–1.0 km). This apparently is why measurements of vertical gradients in the atmosphere and lower ionosphere (a height interval from 50 to 120 km) have not

Received: 15 June 2002 / Accepted: 13 August 2002
Published online: 11 October 2002
© Springer-Verlag 2002

A. Pavelyev · Y.-A. Liou (✉) · C.-Y. Huang
Center for Space and Remote Sensing Research,
National Central University, Chung-Li 320, Taiwan
E-mail: yueian@csrr.ncu.edu.tw
Tel.: +886-3-4227151
Fax: +886-3-4254908

A. Pavelyev
Institute of Radio Engineering and Electronics of Russian
Academy of Sciences (IRE RAS), Fryazino, Vvedenskogo Sq. 1,
141120 Moscow, Russia

C. Reigber · J. Wickert
GeoForschungsZentrum Potsdam,
Telegrafenberg, 14473 Potsdam, Germany

K. Igarashi · K. Hocke
Communication Research Laboratory,
Independent Administrative Institute,
4-2-1 Nukui-Kita Machi, Koganei-shi, Tokyo 184-8795, Japan

been used in most RO work, with some rare exceptions (Vorob'ev et al. 1999; Sokolovskiy 2000; Igarashi et al. 2000, 2001; Liou et al. 2002; Pavelyev et al. 2002a, 2002b). Also, reflections from the Earth's surface have not been considered in GPS/MET RO works up to 2001. To achieve better vertical resolution, a back-propagation method has been proposed. This method is based on the Vladimirov equation (Gorbunov et al. 1996, 2001). Pavelyev (1998), Hocke et al. (1999), and Igarashi et al. (2000) proposed a radio-holographic method based on a focused synthetic aperture approach to obtain extreme high vertical resolution. Igarashi et al. (2001), and Beyerle and Hocke (2001) demonstrated the high vertical resolution of the radio-holographic method (about 20–70 m) through the retrieval of weak signals reflected from the sea surface in the GPS/MET RO data. Beyerle and Hocke (2001) carried out a systematic radio-holographic investigation of the reflected signals in the GPS/MET data to measure the humidity of the atmospheric boundary layer. In future, combination of GPS RO data and a new area of the GPS reflection may provide a simple measurement tool for global observation of the interaction of ocean-atmosphere-ionosphere (Tyler 1966; Pavelyev et al. 1996; Komjathy et al. 1999; Beyerle and Hocke 2001). In addition, Igarashi et al. (2000, 2001, 2002), Pavelyev et al. (2002a, 2002b), and Liou et al. (2002) indicated a new possibility to use the amplitude variations in the RO signals to retrieve the vertical electron-density gradients in the lower ionosphere and temperature in the atmosphere.

Our aim in this paper is to present a short review of new radio-holographic methods, including their applications to the three- and two-dimensional cases, inhomogeneous medium, to describe their connection with the focused synthetic aperture approach, and to demonstrate that the amplitude data of RO signals can be used (in addition to the phase data) to retrieve the gradients of the electron density in the mesosphere and refractivity in the atmosphere.

Radio-holographic equations

The geometry of the radio-holographic and the radio-occultation scheme is shown in Fig. 1. The GPS transmitter and the receiver are located correspondingly at points G and P, respectively, at distances R_2 and R_1 from the center of spherical symmetry (point O). The angle between directions OG and OP is denoted θ . Point D is the specular reflection point on a smooth sphere of radius a corresponding to the average Earth surface. The direct and reflected signals propagate through different parts of the ionosphere and atmosphere along paths GP and GDP. The receiver on the LEO satellite registers the phase and amplitude of the radio waves along the LEO trajectory SP at two frequencies (F_1 and F_2) corresponding to wavelengths of 19 and 24 cm (L_1 and L_2), respectively. Thus, two radio holograms were obtained during every event of the RO experiments. Generalization of the radio-holography approach consists of application of the vector equation given by Stratton and Chu (Stratton 1941) for a back-propagated field (Pavelyev et al. 2001) and an inhomogeneous medium. Vector equations for the radio-holographic method have been obtained in the form (for the Gauss units system)

$$E(A) = ik(4\pi)^{-1} \iint dS Q_E(E, H); Q_E(E, H) = \{(n \times H)\phi + [(n \times E) \times \nabla\phi + (n \cdot E)\nabla\phi]/(ik)\}, \quad (1)$$

$$H(A) = ik(4\pi)^{-1} \iint dS Q_H(E, H); Q_H(E, H) = \{(n \times E)\phi - [(n \times H) \times \nabla\phi - (n \cdot H)\nabla\phi]/(ik)\}, \quad (2)$$

where $E(x', y', z')$ and $H(x', y', z')$ are the backward propagation electromagnetic fields at an interior observation point $A(r')$ (Fig. 1) of the inhomogeneous medium in terms of known values of E and H over a surface S, $\phi(r-r')$ is the Green function corresponding to a backward propagation field, and r determines coordinates of the current

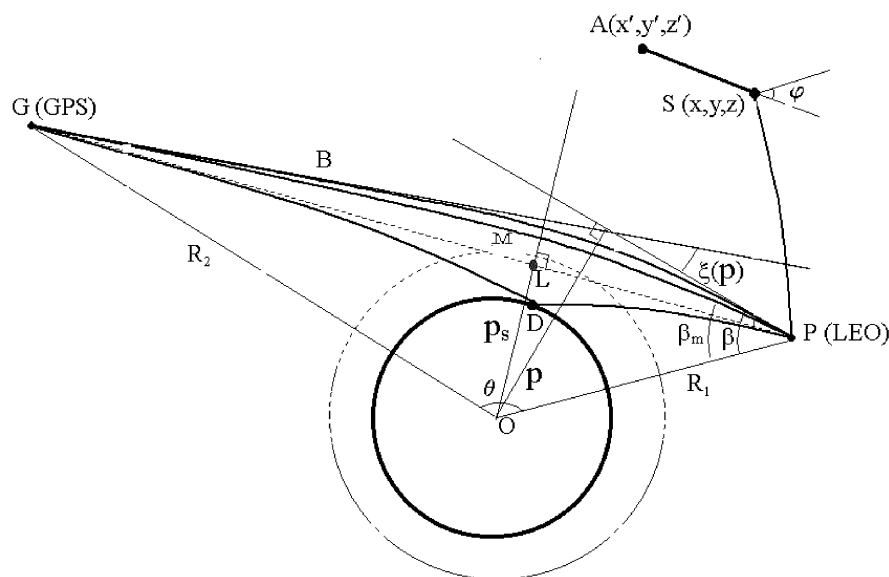


Fig. 1
Scheme of the radio occultation experiment

integration point. The Green function ϕ can be obtained from a wave equation for an inhomogeneous medium:

$$\Delta\phi + k^2\phi = \delta(r - r'), \quad k = n(r)k_0, \quad (3)$$

where $\delta(r-r')$ is a delta-function, k_0 is the free space wave number, and $n(r)$ is the refraction index within which the absorption effect is accounted for. Equations (1) and (2) give a general presentation for backward propagation fields, if the fields on some surface S are known and the point of observation A is located inside the inhomogeneous medium. Intersection of the interface S with plane PGO is shown by the line PS . To determine the backward propagation field, we must find the Green function ϕ by solving the wave Eq. (3). The wave Eq. (3) has two solutions: ϕ_a and ϕ_b which correspond to direct and back propagation radio waves, respectively. For an inhomogeneous medium, under some assumptions, the physical optics approximation may be used and a solution of Eq. (3) ϕ may be found in the form (Kravtsov and Orlov 1990)

$$\phi_{a,b} = A_{\pm} e^{\pm i\Phi} / r; \quad \Phi = k_0 \int n dl, \quad (4)$$

where Φ and A_{\pm} are the phase and amplitude of the Green functions corresponding to direct (index “+”) and backward (index “-”) propagation waves, k_0 is the free space wave number, and n is the refraction index within which the absorption effect is accounted for. The integration in Eq. (4) is provided along the ray connecting the observation point $A(x', y', z')$ and element ds on the surface S . For a homogeneous medium $\Phi = kr$ and $A_{\pm} = 1$, so we can obtain from Eq. (3)

$$\phi = e^{-ikr} / r, \quad r = |r - r'| \quad (5)$$

for the time dependence of the field assumed in the form $\exp(-i\omega t)$, where ω is the angular frequency. Equations (1) and (2) are the basic radio-holography equations for a three-dimensional case, and can be used to reconstruct the electromagnetic field inside the homogeneous part of the space between the atmosphere and LEO satellite, if the fields E and H are known at interface S . Note that information on the field distribution on some part of the surface S can be used to construct an image of refractive volume as follows from holographic practice used in optics. The spatial resolution depends on the size of the part of interface S where the field distribution is given. We can obtain an equation corresponding to the two-dimensional case by using Eqs. (1) and (2) for the case of local spherical symmetry. As shown by Pavelyev et al. (2001), the field in plane POG, if the LEO satellite moves along a given curve SP (Fig. 1) in the same plane, is described by

$$E(A) = (k/2\pi)^{1/2} \int ds \phi_b \cos \varphi E_0; \\ \phi_b = A_- r^{-1/2} \cos \varphi \exp(i\pi/4 - i\Phi), \quad \Phi = k_0 \int n dl, \quad (6)$$

where φ is the angle between normal to the curve PS and the direction to the point of observation, and ds is an integration element belonging to the curve PS .

Usually the back propagation field $u(x, y, z)$ is calculated using the diffractive integral (Vladimirov 1971; Gorbunov et al. 1996)

$$u(x', y', z') = (k/2\pi)^{1/2} \int ds |r - r'|^{-1/2} \cos \\ \times \varphi \exp(i\pi/4 - ik|r - r'|) u_0(r'), \quad (7)$$

where φ is the angle between vector $r-r'$ and normal to curve SP at the current integration point P , and $u_0(r)$ is a scalar field measured along the orbit of the LEO satellite. Equations (6) and (7) coincide with the homogeneous medium and the scalar case.

Focused synthetic aperture method

For the circular orbits of the GPS and LEO satellites, integration along the LEO trajectory can be replaced in Eq. (6) by integration over time by changing the variables $ds = v dt$, and $v = R_1 d\theta/dt$. The field $E(A)$ in Eq. (6) can be found on the known temporal dependence $E_0(t)$ by transformation:

$$E(A) = (k_0/2\pi)^{1/2} \int dt S_r(t) E_0; \\ S_r(t) = v A_- r^{-1/2} \cos \varphi \exp(i\pi/4 - i\Phi), \quad (8) \\ \Phi = k_0 \int n dl,$$

where r is the distance SA . The function $S_r(t)$ in Eq. (8) may be recognized as a reference signal. The reference signal $S_r(t)$ is the kernel of the radio-holographic transform (Eq. 8). The reference signal $S_r(t)$ in Eq. (8) allows one to convert the known field distribution along a LEO orbit to the field distribution $E(A)$ in a space between the GPS transmitter and LEO receiver. As follows from above, the reference signal $S_r(t)$ in Eq. (8) is proportional to the scalar Green function for a back propagation field. For a homogeneous medium the reference signal is equal to:

$$S_r(t) = v r^{-1/2} \cos \varphi \exp(i\pi/4 - ikr). \quad (9)$$

Pavelyev (1998), Hocke et al. (1999), and Igarashi et al. (2000) proposed a different approach to analyze the RO data. They considered the recorded RO signal $E(t)$ as the radio hologram's envelope which consists of the amplitude $A(t)$ and phase $\psi(t) = kS_e(t)$ of the radio field as functions of time:

$$E(t) = A(t) \exp[-i\Psi(t)]. \quad (10)$$

In addition, they assumed that the recorded signal $E(t)$ may be presented as a superposition of the waves with the complex amplitudes $A_{sj}(\beta, p)$ propagating along the rays at different angles β_j relative to the line PO and having different impact parameters p_j . The fields corresponding to each component of the angular spectrum $A_{sj}(\beta, p)$ are

naturally in coherence with the main ray GP (Fig. 1) because they have a common origin. The reference signal $E_m(t) = A_m^{-1}(t) \exp(i\psi_m(t))$ must be developed to acquire maximum coherence with the RO signal. Thus, the phase $\psi_m(t)$ and amplitude $A_m(t)$ of the reference signal must be related to $\psi_c(t)$ and $A_c(t)$ of the main (coherent) part of the RO signal corresponding to the main ray GP. To achieve this, a model of refractivity in the atmosphere and ionosphere can be applied. Naturally, the model must be representative to the actual physical conditions in the radio-occultation region. Functions $A_m(t)$ and $\psi_m(t)$ determine parameters of the focused synthetic aperture and the spatial resolution. Without such a model, the spatial resolution will correspond to an unfocused synthetic aperture (Doppler selection) and will be roughly 0.5–1 km. Igarashi et al. (2000, 2001) used the amplitude $A_m(t) = \text{const}$ and an exponential model to describe the refractivity profile of the atmosphere with the IRI-95 model for the ionosphere in the RO region to determine the temporal dependence of $\psi_m(t)$, and they obtained a spatial resolution of about 20–70 m. They applied the Fourier transformation to the product of the RO and reference signals to obtain the compressed angular spectrum $A(\beta(\omega), p(\omega))$ of the RO signal:

$$A(\beta(\omega), p(\omega)) = \int_{-\frac{T}{2}}^{\frac{T}{2}} \int dt E(t) A_m^{-1}(t) \exp[i\psi_m(t)] \exp(-i\omega t);$$

$$\sin \beta = \omega / (kv) + \sin \beta_m; \quad p = \omega R_1 / (kv) + p_m;$$

$$k = 2\pi / \lambda; \quad v = R_1 d\theta / dt, \quad (11)$$

where β is the angle between direction PO and the tangent to ray GBP at point P (Fig. 1), β_m is the angle β , p_m is the impact parameter p corresponding to the trajectory GMP of the reference signal at point P (Fig. 1), and T is the time of coherent data analysis. Equation (11) describes the angular spectrum of the radio field $A(\beta(\omega), p(\omega))$ as a function of ray coordinates β and p . The second and third parts of Eq. (11) permit an independent measurement of the impact parameters p , p_m and refraction angles $\xi(p)$, $\xi(p_m)$ corresponding to each ray in the angular spectrum $A(\beta, p)$ (Hocke et al. 1999; Igarashi et al. 2000; Pavelyev et al. 2002a, 2002b).

From a formal point of view, there is a similarity between Eqs. (8) and (11). In Eq. (8) the reference signal $S_r(t)$ from Eq. (9) is used to find the field distribution $E(A)$. In Eq. (11) the angular spectrum $A(\beta(\omega), p(\omega))$ is determined as a Fourier transformation of the product of the reference signal $E_m(t)$ and the known field $E(t)$. Eq. (11) gives also an estimate of the field near transmitter G because if $\omega=0$ then Eq. (11) coincides with Eq. (8) if $R_d = PG$. This means that the synthetic aperture is focused at point G. Thus, the method of the focused synthetic aperture directly gives a solution of the RO inverse problem: to find the temporal dependencies of the amplitude, phase, impact parameter, and refraction angle for each ray in the angular spectrum of the radio field. Equation (8) does not directly give a solution of the RO inverse problem because it is necessary to have special algorithms to find the refraction

angle and impact parameter on the field distribution $E(A)$. This problem has been considered in publications devoted to analysis of the RO data by the back propagation method (e.g., Mortensen and Hoeg 1998; Gorbunov et al. 2001). The vertical resolution of the focused synthetic aperture method, $\Delta h \approx \lambda R_1 / (2vT)$, is essentially higher than that corresponding to the unfocused synthetic aperture $\Delta h \approx (\lambda R_1)^{1/2}$. Using the focused synthetic aperture approach, Igarashi et al. (2001) obtained a series of radio images of the Earth's limb (i.e., radio brightness distributions along the straight line OL in Fig. 1) as seen from a LEO satellite.

Examples of the radio images of the atmosphere and the Earth's surface in the RO region are shown in Figs. 2 and 3. These data relate to RO event no. 0392 (5 February 1997; 13 h 54 min 42 s UT; 55.6°N, 139.2°E). The radio image of the mesosphere near 56.5 km (Fig. 2) contains one sharp spike because there is a single-ray propagation mode. The vertical width of the spike is about 50–70 m. It corresponds to an angular resolution of about 17–23 microradian. The broadening of the angular spectrum in the upper atmosphere may be related to the effects of turbulence. The radio brightness distribution in the boundary layer at a height of 1 km is shown in Fig. 3. One pixel in the angular spectrum corresponds to a 0.004-microradian variation in the arrival angle, and a 12-m change in the minimum height of the ray above the terrestrial surface. Negative-height values correspond to the signals reflected from the Earth's surface. The main peak corresponds to a radio-occultation signal propagating along the path GBP (Fig. 1). Also, a very broad pedestal is seen in Fig. 3. This part of the radio image corresponds to a conjunction of the reflected and tropospheric signals in the boundary layer. The intensity of the pedestal is compared with the

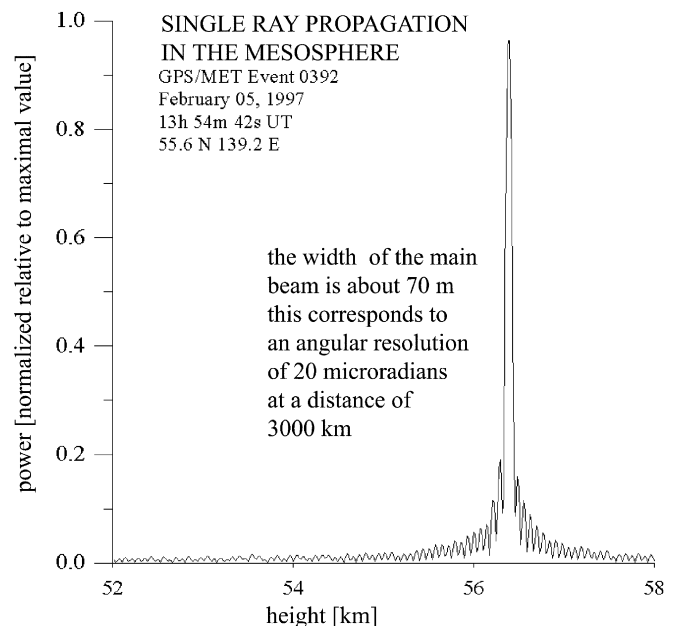


Fig. 2

A radio image of the mesosphere at height 56 km. Radio brightness distribution is sharp due to single-mode propagation

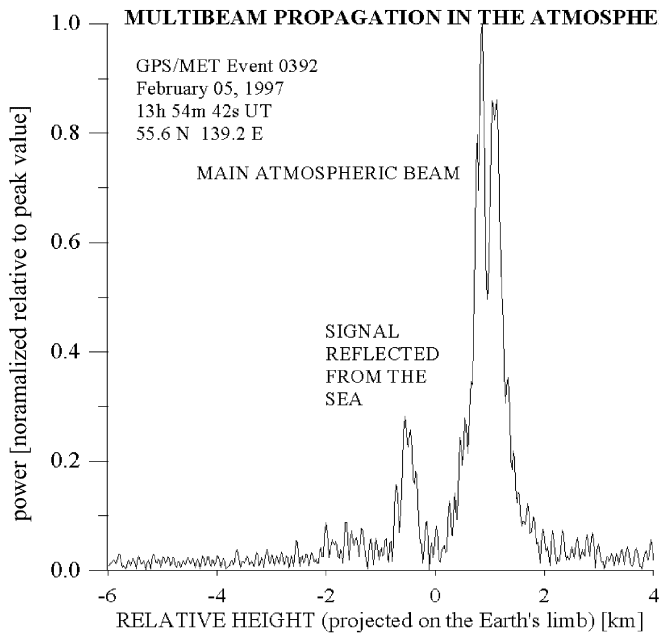


Fig. 3

Projection of the radio image of the atmosphere and the sea surface on the line OL (Fig. 1). Negative heights correspond to reflected signals

level of signal of the main ray. It follows from Figs. 2 and 3 that the radio holographic-focused synthetic aperture method may resolve in detail the one-dimensional vertical radio images of the atmosphere with a scale of 20–50 m, which corresponds to a spatial resolution of about 1/10 of the Fresnel zone size.

Retrieving vertical gradients of refractivity, temperature and electron density

As follows from above, a focused synthetic aperture approach is convenient to detect multi-beam propagation in the atmosphere and ionosphere. Thus, this method may be used to select the RO events with the single wave propagation modes. In the case of single wave propagation, the amplitude and phase of the RO signal may be considered as two independent information channels of radio holograms at frequencies $F1$ and $F2$. Amplitude variations of the GPS signals may be used to obtain altitude distribution of the vertical gradient of the refractivity. The impact parameter p of the main ray (Fig. 1) is connected with the energy of the GPS RO signal (Pavelyev et al. 1986):

$$p(t) - p(t_0) = \int_{t_0}^t dt X[t(p_s)] - X_m[t(p_s)] dp_s / dt \quad (12)$$

where X_m and X are the power attenuation of the GPS RO signals relative to free space owing to the refraction effect for the model of the atmosphere in the RO region and the

experimental data, respectively. Equation (12) allows one to find the temporal dependence of the impact parameter $p(t)$ from the amplitude data using the deflections of the experimental data from the simulation (model) results if the initial conditions are given. The power attenuation $X(t)$ is connected with derivative of the refraction angle on impact parameter $d\xi/dp$

$$d\xi/dp - d\xi_m/dp = X_m(t)^{-1} [1 - X_m(t)/X(t)] B(p_s);$$

$$B(p) = (R_1^2 - p^2)^{-1/2} + (R_2^2 - p^2)^{-1/2}, \quad (13)$$

where the derivative $d\xi_m/dp$ corresponds to the model of atmospheric refraction. Thus, the amplitude data may be used to restore the impact parameter $p(t)$, refraction angle $\xi(t)$ (Eq. 12) and derivative $d\xi/dp(t)$ independently from the phase channel. These temporal dependencies may be used to find the vertical distribution of the refractivity gradient $dN(h)/dh$

$$J(p) = 1/\pi \int_p^\infty d\xi'_x(x)/dx (x^2 - p^2)^{1/2} dx;$$

$$N'_h(h) = -n^2(h)J(p)/\{p[1 + J(p)]\}; \quad (14)$$

As shown by Pavelyev et al. (2001), a connection exists between the vertical temperature and refractivity gradient

$$[dT_w(h)/dh]/T_w(h) = -[N(h)]^{-1} dN(h)/dh - T_x/T_o(h),$$

$$T_x = 34.05 \text{ K/km}. \quad (15)$$

Equation (15) connects the vertical gradient of the logarithm of the refractivity with the vertical gradient of the logarithm of the “wet” temperature $T_w(h)$. Equations (14) and (15) allow one to retrieve the vertical gradients of the refractivity and temperature from the variations of the amplitude of GPS signals after propagation through the atmosphere. Note that a method to obtain the vertical temperature and electron-density profiles from amplitude data, which is similar to our approach in some details, has been reported also by Sokolovskiy (2000). The main distinction is that we use a model to control the multi-beam and diffraction effects, and directly apply our exact solution of the inverse problem (Pavelyev et al. 1986) to obtain detailed vertical profiles of the vertical gradients of the refractivity and the physical parameters of the atmosphere and ionosphere. This allows us to obtain new information concerning the vertical temperature gradient in the atmosphere.

The radio-holographic approach described above has been used to analyze the amplitude RO data. Experimental data are shown by curves A1 and A2 in Fig. 4 for GPS/MET RO event 0393 (14 February 1997). The amplitudes corresponding to the reference signals at two wavelengths L1 and L2 are described by the smooth curves M1 and M2 in Fig. 4. (curves A2 and M2 are displaced for comparison). The amplitudes M1 and M2 were obtained through numerical ray tracing using the model of electron density $N_m(h)$ and its gradient $dN_m(h)/dh$ (curves 2 and 4 in

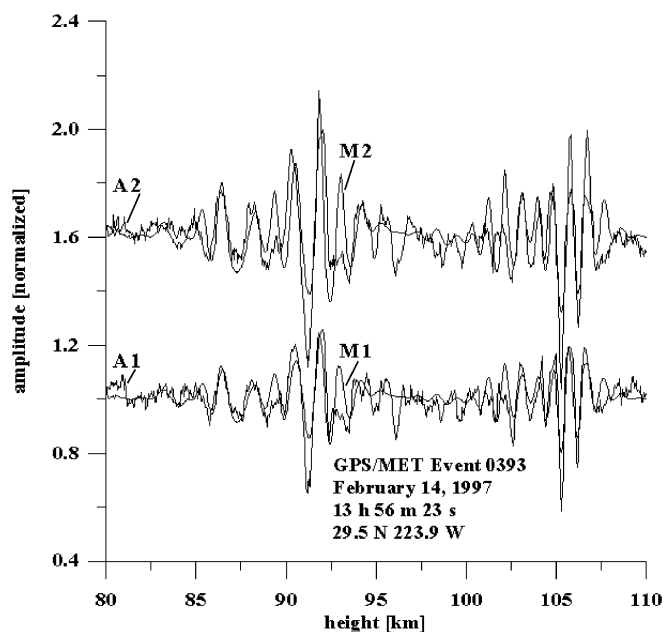


Fig. 4
A comparison of the amplitude variations A1 and A2 at two frequencies with amplitudes of the reference signal (*continuous curves M2, M1*)

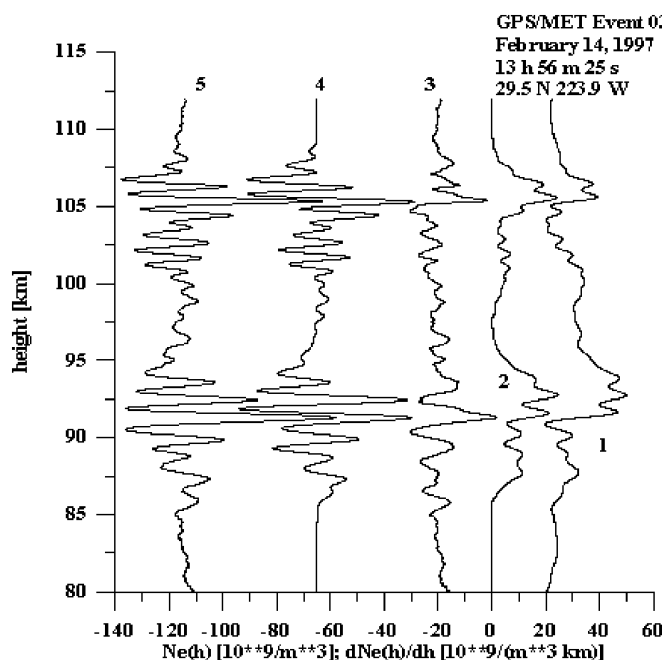


Fig. 5
Results of the restored vertical distribution of the electron density $N_e(h)$ and its gradient $dN_e(h)/dh$. Curves 1, 3, 4, and 5 are displaced by 20 (10^9 m^{-3}), -20, -65, and -115 ($10^9 \text{ m}^3 \text{ km}^{-1}$) correspondingly for comparison. Curves 2 and 5 described model $N_m(h)$, dN_m/dh , used to calculate the curves M1 and M2 in Fig. 4 (*left panel*). Curves 1 and 4 described $N_e(h)$, dN_e/dh retrieved from the RO data. Curve 3 represents the difference $dN_e/dh - dN_m/dh$

Fig. 5). There was a satisfactory correspondence between the amplitudes of the reference signals and the experimental data. Features at heights of 92 and 105 km

corresponding to the sporadic E-layers are clearly seen in both the experimental and computed data. The method described above was used to obtain the vertical gradient $dN_e(h)/dh$ (curve 5 in Fig. 5), electron density $N_e(h)$ (curve 1), and the difference $dN_e(h)/dh - dN_m(h)/dh$ (curve 3). The highest positive maximums of $dN_e(h)/dh - 48 \times 10^9$ and $43 \times 10^9 \text{ m}^{-3} \text{ km}^{-1}$ were at 92 and 105 km. The corresponding maximums in the electron density were about $25\text{--}20 \times 10^9 \text{ m}^{-3}$ and occurred at heights 94 and 106 km. Secondary maximums can also be seen in Fig. 5. The results shown in Figs. 4 and 5 indicate the sensitivity of the amplitude channels of the RO signal to variations in the vertical electron-density gradient in a sporadic E-layer of the ionosphere. The vertical gradients of the refractivity in the atmosphere can also be studied by using the amplitude part of the radio hologram of the RO signal. For example, amplitude variations at wavelengths L1 and L2 are shown in Figs. 6 and 7 (curves A1, A2) for RO GPS/MET events 0537 and 0648. These events correspond to 19 June 1995 and describe radio-meteorological conditions near the equator (event 0537) and at moderate latitude (event 0648). The amplitude data A1 and A2 are normalized, scaled by 50 times and displaced for comparison. The amplitude variations are compared with the results of the retrieved vertical gradient of the refractivity $g(h)$ (N units km^{-1}) from the amplitudes A1 and A2 (curves G1+10, G1 and G2-45, G2-50 in Figs. 6 and 7, respectively). Results of the retrieve vertical gradient of refractivity from the phase data obtained by numerical differentiating of UCAR refractivity data are shown also for comparison (curves GU, GU-15 in Figs. 6 and 7). Curves G1, G2, and GU in Figs. 6 and 7 are obtained from the measured gradients of refractivity by subtracting the part corresponding to a standard refractivity profile with exponential depen-

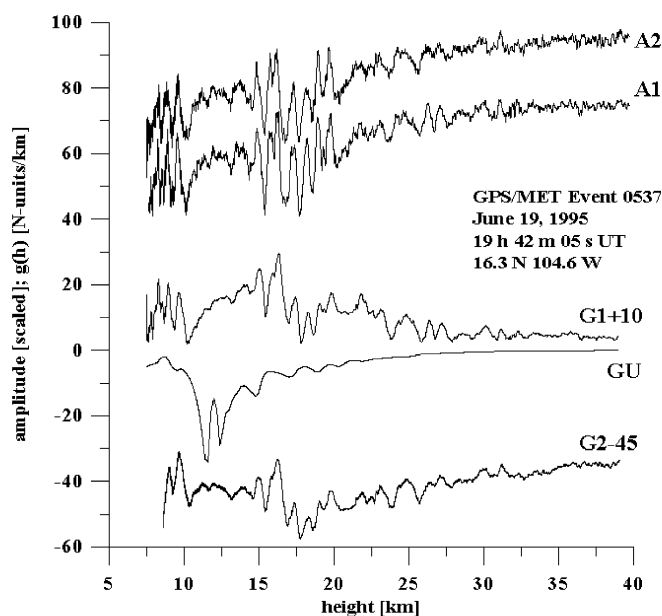


Fig. 6
Wave part of the vertical gradient of the refractivity retrieved from the amplitude channels of the radio holograms at wavelengths L1 and L2 (GPS/MET RO event 0537)

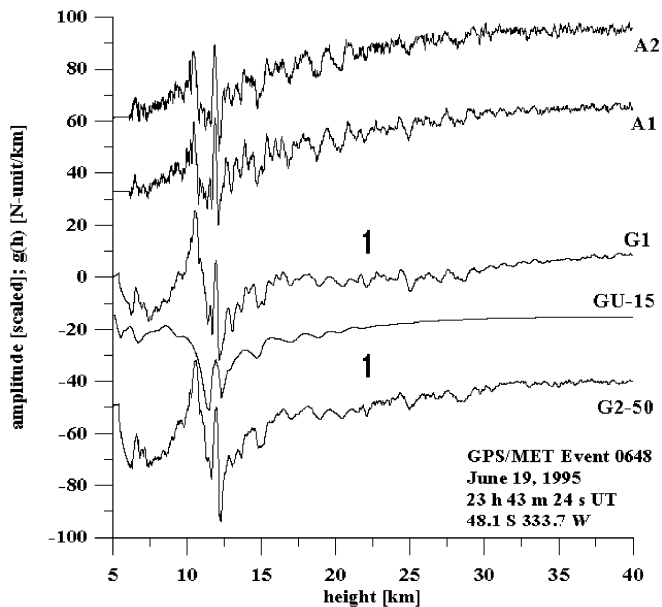


Fig. 7

Wave part of the vertical gradient of refractivity retrieved from the amplitude channels of the radio holograms at wavelengths L1 and L2 (GPS/MET RO event 0648)

dence of refractivity on height: $G(h) = -42 \exp(-0.1265 h)$ ($N \text{ unit km}^{-1}$). These curves are scaled by a factor of 5 in the height interval 5–21.5 km, and by a factor of 20 for the heights above 21.5 km for better comparison with the amplitude data. It can be seen that the vertical gradient of refractivity follows the amplitude variation with some delay, depending on the vertical periods of the amplitude changes. Most essential variations $\pm 2\text{--}5 N \text{ unit km}^{-1}$ are observed near the tropopause level, and can be connected with regular atmospheric processes at the boundary layer between the troposphere and stratosphere. Variations of the vertical gradient of refractivity in the stratosphere are smaller than those in the tropopause region by factors 10–20. However, correspondence to the amplitude variations are clearly seen. Wave structures in the stratosphere can be observed both in amplitude and refractivity data. Results of the UCAR phase retrieval are similar to the low frequency part of the vertical gradient variations restored from the amplitude data analysis. High-frequency components of the spatial variations can be better seen in the vertical gradient of the refractivity obtained from the amplitude data. This can be seen also from the results of restored vertical temperature profiles from the amplitude data. These results are shown in Figs. 8 and 9 for RO events 0537 and 0648, respectively. Curves T1 and T2 in Figs. 8 and 9 (displaced by $\pm 20 \text{ K}$ for comparison) indicate the temperature vertical profiles retrieved from the amplitude data A1 and A2 by integrating the vertical gradient $dT(h)/dh$. Curve TU in Figs. 8 and 9 indicates UCAR temperature retrieved from the phase RO data. Curve TA (displaced by -10 K) corresponds to an average of T1 and T2: $TA = (T1 + T2)/2$. Curve TS is obtained by a smooth approximation of the UCAR temperature and describes the background temperature profile.

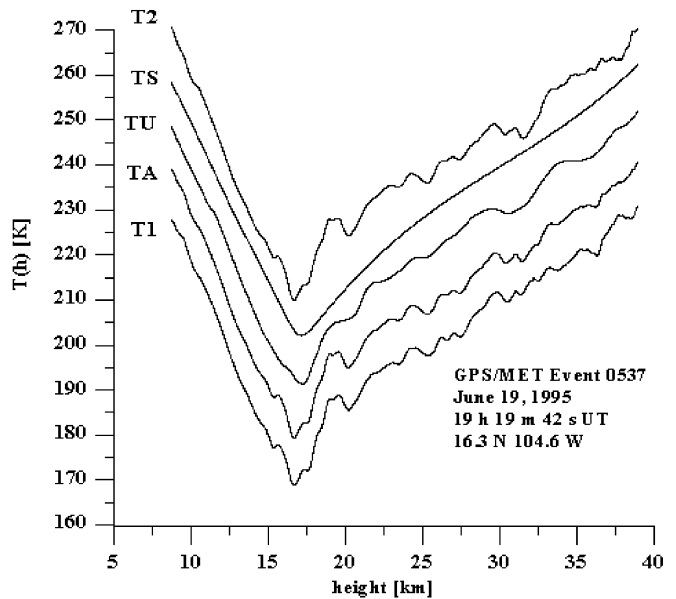


Fig. 8

Temperature vertical profiles restored from the amplitude channels of the radio holograms at wavelengths L1 and L2 (GPS/MET RO event 0537)

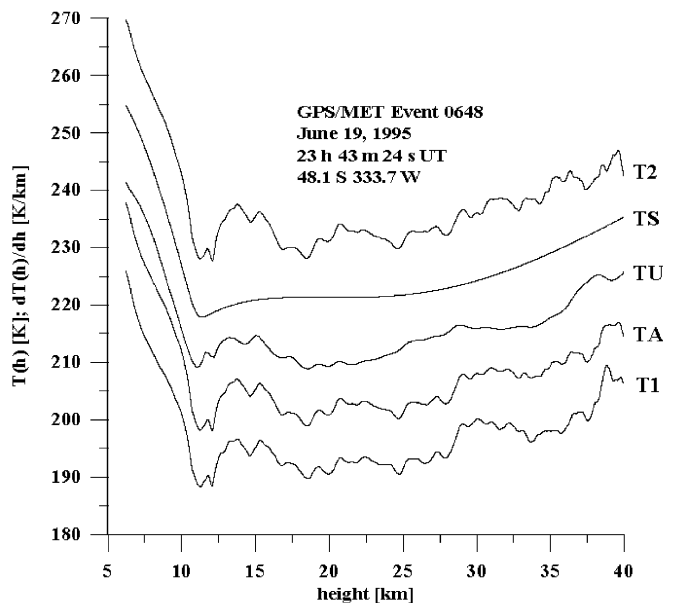


Fig. 9

Temperature vertical profiles restored from the amplitude channels of the radio holograms at wavelengths L1 and L2 (GPS/MET RO event 0648)

Comparing Figs. 8 and 9 demonstrates different physical conditions in the moderate latitude and equatorial atmosphere. The tropopause height increases from 11 km for the moderate latitude up to 17.5 km in the equatorial atmosphere. The slope of the temperature profile in the equatorial atmosphere is of about 2 times higher. A general feature is the wave structures, which are clearly seen above the tropopause level. Amplitude of the temperature variations connected with the waves structures is about

5–8 K and the vertical period is about 1–5 km. The wave structures are more clearly seen in the vertical profiles of $dT(h)/dh$ shown in Figs. 10 and 11. Curves 1 and 2 show the wave part of the temperature variations: TA–TS and TU–TS (K). Curve 1 is displaced by 5 K for comparison. Curves 3 (UCAR data) and 4 (amplitude data) demonstrate the wave part of the temperature vertical gradient $dT(h)/dh$ obtained by subtracting the vertical gradient corresponding to the background temperature from experimental values of $dT(h)/dh$. Curve 3 describes the temperature gradient restored via the numerical differentiation of the UCAR temperature profile. Vertical gradients obtained from the amplitude data show more essential variations in the high-frequency part of spatial spectra than the vertical temperature gradient restored from UCAR temperature (phase data). This discrepancy corresponds to a high sensitivity of the RO amplitude signal to temperature variations in the atmosphere. The low-frequency part of height dependence of the vertical gradients $dT(h)/dh$ is in a good agreement with the vertical gradient retrieved from UCAR temperature profile. Variations of the vertical gradient in the stratosphere revealed wave-like structures with vertical periods of about 0.8 to 4 km, and amplitude of about ± 4 to 6 K km^{-1} . Observation of the vertical gradients of refractivity in the tropopause by means of analysis of the amplitude variations in the RO signal shows the usefulness of the suggested method to study natural processes in the atmosphere.

Conclusions

As follows from a short review, GPS radio holography realizes the high precision of the GPS radio signals for

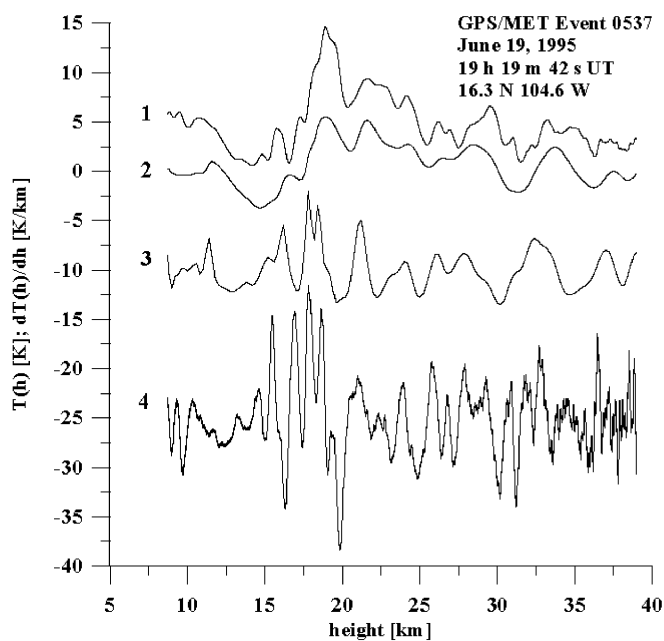


Fig. 10 Wave part of the vertical profiles $T(h)$ and $dT(h)/dh$ (GPS/MET RO 0537)

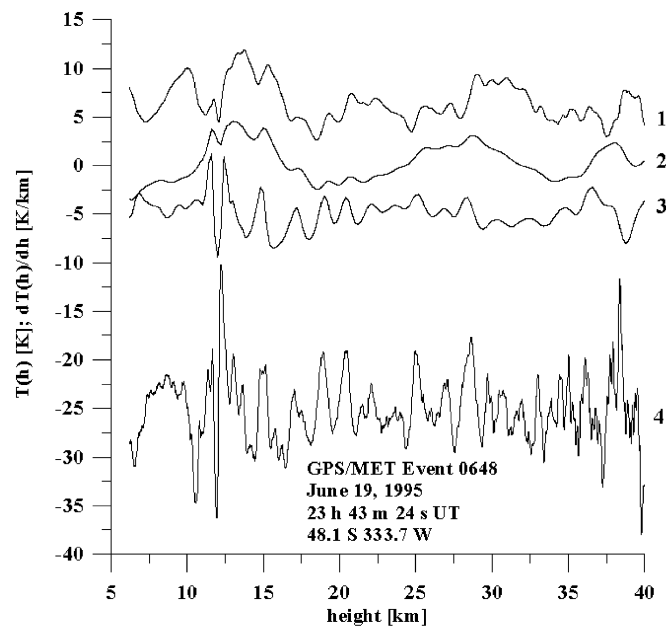


Fig. 11 Wave part of the vertical profiles $T(h)$ and $dT(h)/dh$ (GPS/MET RO 0648)

remote sensing of the atmosphere, mesosphere and terrestrial surface with high spatial resolution and accuracy. Different kinds of radio-holography equations have been considered. A simplified two-dimensional vector equation of the radio-holographic method developed under an assumption of local spherical symmetry can be used to obtain vertical profiles of refractivity in the atmosphere and electron density in the ionosphere, and two-dimensional radio images of the atmosphere and terrestrial surface with a vertical resolution of about 70 m. Application of the new amplitude method to analyze the RO data gives detailed vertical profiles of the temperature and its gradient in the atmosphere in the height interval 5–40 km. Fine structures in the vertical gradient of the electron density have been retrieved from the RO amplitude radio-holographic channels in the sporadic E-layers (height interval 92–105 km). This demonstrates that the GPS radio holography can be used for detailed measurements of the atmospheric and ionospheric parameters in the future COSMIC RO mission.

Acknowledgments We are grateful to UCAR for access to the GPS/MET data. We are grateful to the National Science Council of Taiwan, R.O.C. for financial support under grants NSC 91-2811-M008-001, NSC 90-2111-M008-047-AGC, and the Office of Naval Research (ONR), U.S.A. under grant N00014-00-0528. The work has been partially supported by the Russian Fund of Basic Research, grant 01-02-17649.

References

- Beyerle G, Hocke K (2001) Observation and simulation of direct and reflected GPS signals in radio occultation experiments. *Geophys Res Lett* 28(9):1895–1898

- Feng DD, Herman BM (1999) Remotely sensing the Earth's atmosphere using the Global Positioning System (GPS) – the GPS/MET data analysis. *J Atmos Ocean Technol* 16:990–1002
- Gorbunov ME (2001) Radio holographic methods for processing RO data in multipath regions. Danish Meteorological Institute (DMI) Copenhagen Sci Rep 01-02
- Gorbunov ME, Gurvich AS, Bengtsson L (1996) Advanced algorithms of inversion of GPS=MET satellite data and their application to reconstruction of temperature and humidity. Max-Planck-Institute for Meteorology Rep 211
- Hajj GA, Romans LJ (1998) Ionospheric electron density profiles obtained with the Global Positioning System: results from GPS/MET experiment. *Radio Sci* 33(1):175–190
- Hocke K, Pavelyev A, Yakovlev O, Barthes, Jakowski N (1999) RO data analysis by radio holographic method. *JASTP* 61:1169–1177
- Igarashi K, Pavelyev A, Hocke K, Pavelyev D, Kucherjavenkov IA, Matugov S, Zakharov A, Yakovlev O (2000) Radio holographic principle for observing natural processes in the atmosphere and retrieving meteorological parameters from RO data. *Earth Planet Space* 52:968–875
- Igarashi K, Pavelyev A, Hocke K, Pavelyev D, Wickert J (2001) Observation of wave structures in the upper atmosphere by means of radio holographic analysis of the RO data. *Adv Space Res* 27(6–7):1321–1327
- Igarashi K, Pavelyev A, Wickert J, Hocke K, Pavelyev D (2002) Application of radio holographic method for observation of altitude variations of the electron density in the mesosphere/lower thermosphere using GPS/MET RO data. *JASTP* 64 (in press)
- Komjathy A, Garrison JL, Zavorothy V (1999) GPS: a new tool for ocean science. *GPS World* April:50–56
- Kravtsov Y, Orlov YN (1990) Geometrical optics of inhomogeneous media. Springer, Berlin Heidelberg New York
- Kursinski ER, Hajj GA, Schofield JT, Linfield RP, Hardy KR (1997) Observing Earth's atmosphere with radio occultation measurements using the Global Positioning System. *J Geophys Res* 102:23,429–23,465
- Liou YA, Huang CY (2002) Active limb sounding of atmospheric refractivity and dry temperature profiles by GPS/Met occultation. In: L-H Lyu (ed) *Space weather study using multipoint techniques*. COSPAR Coll Ser, vol 12
- Liou YA, Pavelyev AG, Huang CY, Igarashi K, Hocke K (2002) Simultaneous observation of the vertical gradients of refractivity in the atmosphere and electron density in the lower ionosphere by radio occultation amplitude method. *Geophys Res Lett* 29 (in press)
- Mortensen MD, Hoeg P (1998) Inversion of GPS occultation measurements using Fresnel diffraction theory. *Geophys Res Lett* 25(13):2441–2449
- Pavelyev A (1998) On the possibility of radio holographic investigation on communication link satellite-to-satellite. *J Communications Technol Electronics* 43(8):126–131
- Pavelyev A, Matugov S, Kalashnikov I, Yakovlev O (1986) Analysis of the features of radio occultation method for the Earth's atmosphere study (in Russian). In: Sokolov AV, Semenov AA (eds) *Electromagnetic waves in the atmosphere and space*. Nauka, Moscow, pp 208–218
- Pavelyev A, Volkov AV, Zakharov AI, Krytikh SA, Kucherjavenkov AI (1996) Bistatic radar as a tool for earth investigation using small satellites. *Acta Astron* 39:721–730
- Pavelyev A, Yakovlev OI, Matyugov SS, Pavelyev D, Anufriev VA (2001) Advanced algorithms of inversion of GPS radio limb sounding data. *GeoForschungZentrum Potsdam Sci Tech Rep STR01/06*
- Pavelyev A, Yakovlev OI, Matyugov SS, Pavelyev D, Anufriev VA (2002a) Radio holographic analysis of RO data. *GeoForschungZentrum Potsdam Sci Tech Rep 02/05*
- Pavelyev A, Igarashi K, Reigber C, Hocke K, Wickert J, Beyerle G, Matyugov S, Kucherjavenkov A, Pavelyev D, Yakovlev OI (2002b) First application of the radio holographic method to wave observations in the upper atmosphere. *Radio Sci* (in press)
- Rocken C et al. (1997) Analysis and validation of GPS/MET data in the neutral atmosphere. *J Geophys Res* 102(D25):29,849–29,866
- Sokolovskiy SV (2000) Inversion of radio occultation amplitude data. *Radio Sci* 35(12):97–105
- Stratton JW (1941) *Electromagnetic theory*. McGraw-Hill, New York
- Tyler GL (1966) Bistatic radar imaging and measurements techniques for the study of planetary surfaces. PhD Thesis, Stanford University, Stanford, California
- Vladimirov VS (1971) *Equations of mathematical physics*. Pure and applied mathematics, vol 3. Dekker, New York
- Vorob'ev VV, Gurvich AS, Kan V, Sokolovskiy SV, Fedorova OV, Shmakov AV (1999) Structure of the ionosphere from the radio-occultation GPS-“Microlab-1” satellite data: preliminary results. *Earth Observ Remote Sensing* 15:609–622
- Ware R et al. (1996) GPS sounding of the atmosphere from low Earth orbit – preliminary results. *Bull Am Meteorol Soc* 77:19–40